Faraday Discussions

Accepted Manuscript

This manuscript will be presented and discussed at a forthcoming Faraday Discussion meeting. All delegates can contribute to the discussion which will be included in the final volume.

Register now to attend! Full details of all upcoming meetings: http://rsc.li/fd-upcoming-meetings

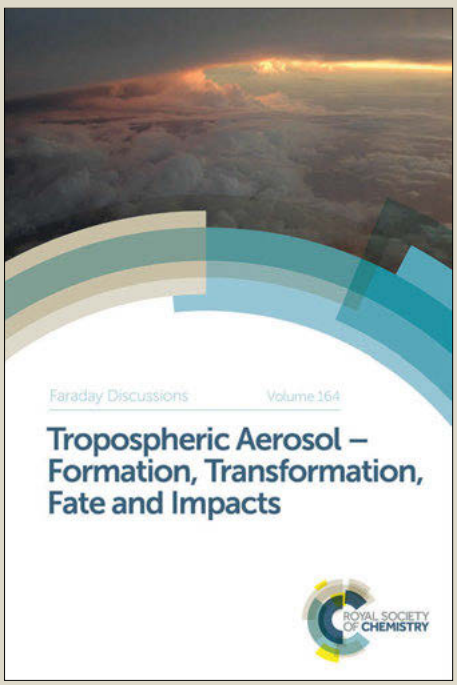

This is an *Accepted Manuscript*, which has been through the Royal Society of Chemistry peer review process and has been accepted for publication.

Accepted Manuscripts are published online shortly after acceptance, before technical editing, formatting and proof reading. Using this free service, authors can make their results available to the community, in citable form, before we publish the edited article. We will replace this *Accepted Manuscript* with the edited and formatted *Advance Article* as soon as it is available.

You can find more information about *Accepted Manuscripts* in the Information for Authors.

Please note that technical editing may introduce minor changes to the text and/or graphics, which may alter content. The journal's standard Terms & Conditions and the Ethical guidelines still apply. In no event shall the Royal Society of Chemistry be held responsible for any errors or omissions in this *Accepted Manuscript* or any consequences arising from the use of any information it contains.

ROYAL SOCIETY OF CHEMISTRY

www.rsc.org/faraday_d

Faraday Discussions

RSCPublishing

ARTICLE

Polycyclic Aromatic Hydrocarbons – Catalysts for Molecular Hydrogen Formation.

Cite this: DOI: 10.1039/x0xx00000x

A.L. Skov,[a] J. D. Thrower[a,b] and L. Hornekær[a]

Received 17th December 2013,
Accepted 00th January 2014

DOI: 10.1039/x0xx00000x

www.rsc.org/

Polycyclic aromatic hydrocarbons have been shown to catalyse molecular hydrogen formation. The process occurs via atomic hydrogen addition reactions leading to the formation of super-hydrogenated PAH species, followed by molecular hydrogen forming abstraction reactions. Here, we combine quadrupole mass spectrometry data with kinetic simulations to follow the addition of deuterium atoms to the PAH molecule coronene. When exposed to sufficiently large D-atom fluences, coronene is observed to be driven towards the completely deuterated state ($C_{24}D_{36}$) with the mass distribution peaking at 358 amu just below the peak mass of 360 amu. Kinetic models reproduce the experimental observations for an abstraction cross-section of σ_{abs} = 0.01 Å^2 per excess H/D atom and addition cross-sections in the range of σ_{add} = 0.55-2.0 Å^2 for all degrees of hydrogenation. These findings indicate that the cross-section for addition does not scale with the number of available sites for addition on the molecule, but rather has a fairly constant value over a large interval of super-hydrogenation levels.

Introduction

Polycyclic aromatic hydrocarbons are ubiquitous in the interstellar medium (ISM) [1] and are believed to play an important role in determining a range of physical parameters, such as the ionization fraction and heating rates in the ISM [1], as well as influencing the chemical composition of the ISM through catalysis of chemical reactions [1-12].

Specifically, observations have suggested that high abundances of PAHs in photo-dissociation/photon-dominated regions (PDRs) are related to high rates of molecular hydrogen formation [2-3]. This has led to the suggestion that PAHs might be involved in H_2 formation in PDRs through chemisorption of H-atoms on PAHs [3]. The presence of such super-hydrogenated PAH species is supported by observations which have revealed aliphatic C–H stretch features at 3.4μm alongside the 3.3 μm aromatic C–H [4-5]. This supports the results of models showing that large PAHs can exist with high degrees of super-hydrogenation in many environments [6]. Although the aliphatic C–H stretch can also arise as a result of the presence of alkane side chains, experimentally obtained IR emission spectra of neutral PAHs with additional peripheral H atoms are more consistent with observations [7].

Theoretical calculations [10-14] and experimental measurements [15-21] strengthen this hypothesis by demonstrating that PAHs may indeed catalyse molecular hydrogen formation. The catalytic activity of both PAH cations and neutrals have been investigated since the charge state of PAHs is strongly dependent on the FUV flux [22]. Furthermore, studies of the catalytic activity of both gas phase and condensed phases of PAH molecules have been conducted mimicking the phase variations between interstellar environments. In diffuse cloud environments PAHs are thought to exist in the gas phase, while in dense clouds IR absorption features attributable to PAHs have been observed toward protostellar objects indicating the presence of both gas [23] and condensed [24] phase PAHs.

The theoretical studies indicate that both PAH cations and neutrals might act as catalysts for H_2 formation [10-14]. This is supported by experimental investigations demonstrating hydrogen addition to gas phase PAH cations [15-17] and to condensed PAH neutrals on grain surfaces [18-20]

In a series of measurements employing surface adsorbed coronene ($C_{24}H_{12}$) as a prototypical PAH which presents three inequivalent binding sites for additional H-atoms, the catalytic activity was observed to proceed via the formation of super-

hydrogenated species, followed by abstraction reactions where excess H-atoms react with incoming H-atoms to form molecular hydrogen [18-19]. Furthermore, it was observed that PAH molecules could abstract H-atoms chemisorbed on the underlying graphite surface [21]. Infrared spectroscopy measurements using a 300 K H-atom beam were used to derive a cross-section for addition of $\sigma_{add} = 1.1$ Å^2 and a cross-section for abstraction of $\sigma_{abs} = 0.06$ Å^2 for each excess H/D atom on the super-hydrogenated coronene molecule [18], while for higher energy H atom beams, such as the one employed here, a slightly smaller cross-section for the addition of the first H-atom to the coronene molecule of $\sigma_{add,first} = 0.55$ Å^2 was found [19].

Here, we combine quadrupole mass spectrometry data with kinetic simulations to follow the addition of hydrogen atoms to the coronene molecule. We identify addition and abstraction cross-sections for the super-hydrogenated species as a function of the degree of super-hydrogenation yielding a good match between experimental and simulated data. We show that the measured mass distributions are simulated well by a model employing an abstraction cross-section of $\sigma_{abs} = 0.01$ Å^2 per excess H/D atom, a factor of 6 lower than the measured cross-section for 300 K beams, and an addition cross-section which is initially $\sigma_{add} = 0.55$ Å^2, increasing to a plateau value of ca. $\sigma_{add} = 2.0$ Å^2 for intermediate degrees of hydrogenation before falling off to a value around $\sigma_{add} = 1.0$ Å^2 for addition of the final six hydrogen atoms. The findings indicate that the cross-section for addition does not scale with the number of available sites for addition on the molecule, but rather has a fairly constant value over a large interval of super-hydrogenation levels.

Methods

Experimental methods

All measurements were performed in an ultrahigh vacuum (UHV) chamber in which a base pressure of $<1\times10^{-10}$ mbar is routinely obtained. The highly oriented pyrolytic graphite (HOPG; SPI grade 1) substrate was supported in a Ta holder fixed to a water-cooled copper mount. This grade of HOPG is characterised by large grain sizes and a low density of step edges and grain boundaries. Sample heating was performed through electron bombardment on the rear of the sample holder. The HOPG was cleaved with adhesive tape prior to mounting in the UHV chamber and annealed to 1200 K under UHV conditions to remove any residual contaminants. The temperature of the HOPG was measured with a type-C thermocouple secured between the front face of the substrate and the Ta holder. During all depositions a substrate temperature of 290±1 K was maintained.

Coronene ($C_{24}H_{12;}$ Aldrich, sublimed, 99%) films were grown by thermal evaporation from the bulk sample using a home built temperature controlled Knudsen cell type molecular doser. A cell temperature of 438 K was typically used, giving a deposition rate of *ca*. 0.03 monolayer s^{-1} (MLs^{-1}). The distance between the doser and the substrate was minimised to reduce deposition on the Ta holder. A beam of D-atoms was produced using a hot capillary thermal cracker to dissociate D_2 (Air Liquide; N30, >99.9%). A capillary temperature of *ca.* 2300 K was used, yielding a typical D-atom flux of 3×10^{14} cm^{-2} s^{-1} to within a factor of two. This estimate was made by considering the operational parameters (capillary temperature, feed pressure, distance to substrate) of the source [25-26]. D-, rather than H-atoms were used to enable detection of abstraction-addition reactions leading to the replacement of original hydrogen atoms on the coronene molecule with deuterium atoms. Temperature programmed desorption (TPD) measurements were performed by heating the substrate linearly to 1200 K at a rate of 1 K s^{-1} with the aid of a PID controller (Lakeshore Model 340). Desorbing coronene and deuterated coronene species were detected with a quadrupole mass spectrometer (QMS; Extrel CMS LLC) with a cross-beam ionization source. The mass range of this QMS ($m/z = 500$) was sufficient to detect the coronene parent ion ($C_{24}H_{12}^+$; $m/z = 300$) and those of all deuterated species up to the deuterated analogue of perhydrocoronene ($C_{24}D_{36}^+$; $m/z = 360$). This mass range was scanned in 1 s allowing for detection of all deuterated products during an individual TPD measurement.

Simulated Mass Distributions

To extract addition and abstraction cross-sections from the experimental data, kinetic simulations of the evolution of the mass distribution as a function of D-atom fluence are performed. These calculations start with a molecular distribution where all molecules are in the form of coronene ($C_{24}H_{12}$; $m/z = 300$) and the addition of D-atoms with a flux of 3×10^{14} cm^{-2} s^{-1}, as in the experiments, is then considered. The molecular distribution is evaluated through a series of time steps. For each time step, there are three possible reactions that molecules can undergo:

$$C_{24}H_xD_y + D \rightarrow C_{24}H_xD_{y+1} \quad (1)$$

$$C_{24}H_xD_y + D \rightarrow C_{24}H_xD_{y-1} + D_2 \quad (2a)$$
$$C_{24}H_xD_y + D \rightarrow C_{24}H_{x-1}D_y + HD \quad (2b)$$

Where (1) is an addition reaction and (2a) and (2b) are reactions in which the incoming D-atom abstracts a D- or H-atom to form D_2 or HD respectively. The rate for an addition reaction involving a super-hydrogenated coronene molecule with n excess H/D atoms is determined by the D-atom flux and a super-hydrogenation degree dependent cross-section, $\sigma_{add}(n)$, for addition of D atoms to the molecule. Since the cross-section for addition is treated as being only dependent on the number of excess H/D atoms on the molecule, n, it is in essence an average over addition into all available sites on all possible conformers of super-hydrogenated coronene for a given degree of super-hydrogenation. Hence, the simulation is not site specific and provides only an average addition cross-section for a given super-hydrogenation degree. In the case of $n = 0$, where no excess H/D atoms have been added to the coronene molecule, the cross-section derived from previous

measurements on the system [19], $\sigma_{add}(0) = 0.55$ Å^2 is used. For $n > 0$, $\sigma_{ad}(n)$, is a variable parameter. The rate of abstraction reactions scales linearly with the D atom flux, the number of excess H/D atoms already present on the molecule, *n,* and the abstraction cross-section, $\sigma_{ab,}$ for each excess H/D atom. No abstraction reactions are allowed for $n = 0$. i.e. the molecules will always have at least 12 H/D atoms. Two different models have been investigated, where the abstraction cross-section has either been taken to be equal to the abstraction cross-section measured for a 300 K H atom beam, $\sigma_{abs} = 0.06$ Å^2 per excess H/D atom [18] (simulation 1) or has been optimized to give a better fit to the data, (simulation 2 and 3). The cross-sections for both hydrogen isotopes are taken to be equal. When the molecular distribution has evolved for a time period matching the experimental conditions, the final mass distribution is calculated by modifying the masses of the molecular distribution to reflect the correct $^{13}C/^{12}C$ ratio, arising from the natural abundance of ^{13}C in the coronene sample, and by including possible fragmentation in the mass spectrometer ionization process. Fragmentation patterns measured for coronene are used for all super-hydrogenated species, since no information on fragmentation of the super-hydrogenated species is available. The fragmentation leads to the loss of 1 H/D atom in 7.5%, 2 H/D atoms in 9.7%, 3 H/D atoms in 2.8% and 4-5 H/D atoms in less than 1% of all molecules in the distribution.

Results and discussion

To determine cross-sections for the addition of H-atoms to (hydrogenated) coronene as a function of the degree of hydrogenation we prepare a monolayer of coronene by exposing an HOPG surface to the coronene source for 60 s, sufficient to produce a film of the order of 2–3 monolayers thick, followed by annealing to 390 K to desorb the multilayers [11] The coronene monolayer is then exposed to the desired fluence of atomic deuterium and a temperature programmed desorption (TPD) measurement for all masses from 285 amu to 365 amu is carried out. The measured TPD spectra are time integrated and normalized to the total ion count to give the total relative yield for each mass component. Each component contains multiple species since several different conformers exist for each hydrogenation degree and since different hydrogenation degrees can yield the same mass depending on the ratio of hydrogen and deuterium atoms on the molecule. By repeating the measurement for several increasing D-atom fluences, the evolution of the mass distribution with D-atom fluence can be obtained. In the following, the experimental data are compared to a series of simulations employing different strategies for determining addition and/or abstraction cross-sections.

In Figures 1-3 the measured evolution in mass distribution for super-hydrogenated coronene as a function of D-atom exposure is displayed as black columns. The initial mass distribution displayed in panels (a) before any exposure to hydrogen is dominated by the parent coronene molecule (m/z= 300), with minor peaks at mass 301 amu and 302 amu due to the natural abundance of ^{13}C, as well as minor peaks just below mass 300 amu which we ascribe to fragmentation in the QMS ionization region. Following exposure to atomic deuterium we observe a reduction in the desorption yield obtained for the parent ion signal at m/z = 300 and the appearance of peaks corresponding to other higher mass species, which are ascribed to super-hydrogenated coronene species [19]. For intermediate D-atom fluences of $\Phi_D = 1.4 \times 10^{17}$ atoms/cm^2, panels (c), a very broad mass distribution stretching from mass 300 to 350 amu is observed, similar to previous observations [19]. Here we expose the sample to even higher D atom fluences of up to $\Phi_D = 3.1 \times 10^{18}$ atoms/cm^2. For these highest fluences, the mass distribution is observed to narrow and peak at mass 358 amu, with a detectable signal even at 360 amu. Such high masses indicate close to complete super-hydrogenation of coronene involving addition of one excess D-atoms to all carbon atoms in the molecule, including those on the central ring, and exchange of almost all H-atoms on the parent coronene molecule with D-atoms via abstraction reactions. It should be noted that the deuterated analogue of the fully hydrogenated perhydrocoronene molecule ($C_{24}D_{36}$) has a mass of 360 amu, and is thus the upper limit expected.

The experimental data are compared to the simulated mass distributions, grey columns, obtained by using the cross-sections displayed in Table 1. For the simulations in Figure 1 the abstraction cross-section per excess H/D atom (each H/D atom beyond the initial 12 H-atoms), σ_{abs}, was held fixed at the experimentally determined value for a 300 K beam of H-atoms: $\sigma_{abs} = 0.06$ Å^2. The mass distribution at lower masses is observed to be reproduced well by the series of addition cross-sections displayed in Table 1, simulation 1. The addition cross-sections used in this simulation fall into three groups: (i) for small n, $\sigma_{add}(n)$ is small and matches the initial addition cross-section, $\sigma_{add}(0) = 0.55$ Å^2 increasing to $\sigma_{add}(0)$=1.0 Å^2 for addition of the 4th D atom. (ii) For intermediate n, $\sigma_{add}(n)$ is at a larger constant value of $\sigma_{add}(n) = 2.5$ Å^2, while (iii) for n>17, $\sigma_{add}(n)$ drops to a smaller value of $\sigma_{add}(n) = 1.3$ Å^2.

The small value for the addition cross-section at low n reflects the small cross-section for the very first addition reaction, for which an energy barrier of 60 meV is predicted by density functional theory (DFT) calculations [10]. Although these calculations reveal reduced energy barriers for subsequent addition reactions on neighbour sites, the majority of addition sites on the molecule will still have high barriers, thus resulting in an overall small cross-section for the first few addition reactions. The good correspondence between the measured and simulated data obtained for the intermediate hydrogenation regime using a constant cross-section indicates that the overall cross-section for addition reactions does not scale significantly with the number of available sites for addition. Finally, the reduced addition cross-section at hydrogenation levels above n = 17 may be related to a reduced cross-section for addition reactions to the center sites of the molecule once outer edge and edge sites are fully saturated. The agreement between simulated and experimental data at the highest D-atom fluences is not as

good, and the simulated mass distribution is clearly broader than that obtained experimentally. In addition, the simulations show a clear odd-even mass oscillation which is not observed in the experimental data. This odd-even oscillation reflects an almost complete abstraction of all the original H-atoms on the coronene parent molecule. Hence, both the broader distribution and clear odd-even oscillation in the simulated data indicate that the value for the abstraction cross-section employed in the simulations is too high. This discrepancy likely arises from the employed cross-sections being obtained from measurements using a 300 K H atom beam, while in the present experiment 2300 K D atoms are used.

Based on theoretical calculations, very small or even vanishing energy barriers are expected for the abstraction of excess H/D atoms, with quantum dynamical calculations on a simplified version of the system indicating that the energy dependence of the reaction is fairly complex [27]. Hence, at present a detailed treatment of the energy dependence of the abstraction cross-section is not possible. In order to investigate the effect of a possible lower abstraction cross-section on the evolution of the mass distribution simulations using reduced abstraction cross-sections were carried out.

In Figure 2, experimental and simulated mass distributions using the cross-sections given in table 1 under simulation 2 are displayed. An abstraction cross-section of σ_{abs} = 0.01 Å^2 per excess H/D atom was used, since this value reproduces best the mass distributions at long exposures. This abstraction cross-section allows a reasonable match between measured and simulated data over a wide fluence range. Again, the addition cross-sections giving the best simulation of the experimental data fall into three groups: (i) for small n, $\sigma_{add}(n)$ is small and matches the initial addition cross-section, $\sigma_{add}(0)$ = 0.55 Å^2 increasing to $\sigma_{add}(0)$ = 1.0 Å^2 for addition of the 4th D-atom. (ii) For intermediate n, $\sigma_{add}(n)$ is at a larger constant value of $\sigma_{add}(n)$ = 2.0 Å^2, while (iii) for n>17, $\sigma_{add}(n)$ drops to a smaller value of $\sigma_{add}(n)$ = 1.0 Å^2. This simulation is seen to give an overall good agreement between the experimental and simulated mass distributions over the entire fluence interval. However, the odd-even variation appearing in the simulated data for short and intermediate H-atom fluences, is not observed in the experimental data. This could be related to differences in fragmentation in the QMS for odd and even mass H/D atom species, which are not incorporated in the present model.

In Figure 3, the best fit for long exposure times using a constant cross-section per available addition site (i.e. the addition cross-section have been chosen to depend linearly on the number of available sites for hydrogenation: $\sigma_{add}(n)$ = *(24-n)* x 0.15 Å^2, see table 1, simulation 3) is shown. Such models could not reproduce the evolution in the mass distribution over the entire interval of D-atom fluences, indicating that the cross-section for H addition does not scale significantly with the number of available sites. Thus, the set of cross-section values used in simulation 2 yield the best agreement with the experimental mass distributions.

In Figure 4 the evolution of several specific masses as a function of D-atom exposure is displayed and compared to those obtained through the model simulations discussed above. Low masses are seen to initially increase in intensity with D-atom fluence as they are formed through addition reactions. With increasing fluence these masses go through a maximum and decrease as they are further hydrogenated to higher mass species. For the largest fluences, a rise in intensity of the highest mass species, above 350 amu, demonstrates that the system is, under our experimental conditions, driven towards complete hydrogenation. The best fit over a wide range of masses is observed for the model used in simulation 2 (see Fig. 2) (red curve) with a low abstraction cross-section of σ_{abs} = 0.01 Å^2 per excess H/D atom and addition cross-sections ranging from $\sigma_{add}(n)$ = 0.55-2.0 Å^2. Figure 4(f) shows the total ion count, integrated over the entire mass range considered, as a function of D-atoms fluence. The total ion count undergoes a sharp decrease for small fluence, reaching a limiting value of around 25% of the initial value. While the QMS sensitivity may be species dependent, it is unlikely that this effect can account for the observed decay in total ion count. This suggests that up to 75% of the originally deposited coronene molecules may be lost from the surface prior to detection during the TPD. Several factors may be responsible for such a loss. It is known that the superhydrogenated coronene species formed through D-atom addition are less strongly bound to the HOPG surface [19,28]. Furthermore, according to DFT calculations [10], many of the addition reactions are exothermic. The energy released may be sufficient to lead to desorption of the less strongly bound hydrogenated species. As a result, the reported cross-sections must be considered lower limits.

Conclusions

The experimental measurements presented here demonstrate that when exposed to sufficiently large hot D-atom fluences coronene is driven towards the completely deuterated state ($C_{24}D_{36}$, m/z = 360), with the mass distribution peaking at m/z = 358 just below the peak mass of 360. Furthermore, a significant loss of molecules from the surface is observed during the hydrogenation process. This loss could potentially be ascribed to chemi-sputtering. The measured mass distributions are simulated well by a model employing an abstraction cross-section of σ_{abs} = 0.01 Å^2 per excess H/D atom, a factor of 6 lower than the measured cross-section for 300 K beams, and an addition cross-section which is initially at σ_{add} = 0.55 Å^2, increases to a plateau value of ca. σ_{add} = 2.0 Å^2 for intermediate degrees of hydrogenation before falling off to a value around σ_{add} = 1.0 Å^2 for addition of the final six hydrogen atoms. The addition cross-sections thus vary only within a range from $\sigma_{add}(n)$ = 0.55-2.0 Å^2 for all degrees of hydrogenation. These findings are in good agreement with the average addition cross-sections measured for low energy D atom beams of σ_{add} = 1.1 Å^2 and indicate that the cross-section for addition does not scale with the number of available sites for addition on the molecule, but rather has a fairly constant value over a large interval of

super-hydrogenation levels. This may indicate that the incoming D atoms are mobile on the coronene molecule and are able to scan the molecule for available addition sites. Similar behaviour has been observed for hydrogenation of graphite [29].

The presented results extend previous investigations of the hydrogenation and catalytic activity of coronene [9,18,19] by providing experimental evidence of the formation of even higher degrees of super-hydrogenation of coronene via addition reactions. Furthermore, the kinetic simulations have provided quantitative values for the cross-section for addition reactions as a function of the degree of hydrogenation of the coronene molecule. The experimental observation of coronene species with very high degrees of super-hydrogenation indicates that such species could be formed under interstellar conditions, lending support to the interpretation of observations of IR features attributed to super-hydrogenated PAHs [4,5]. Given the presence of neutral PAH species within PDRs, the present results may have implications for H_2 formation in such regions. In particular, the cross-section for molecular hydrogen formation via abstraction reactions obtained from measurements with 300 K H atoms is sufficiently high to explain the observed increased molecular hydrogen formation rates in these regions provided that the PAHs display very high degrees of super-hydrogenation (the cross-section scales with the number of excess H atoms on the molecule) [18]. The data reported here, which suggest that the addition cross-section is largely independent of the degree of hydrogenation, indicate that this may indeed be the case. However, further investigations are needed to determine the average hydrogenation degree of PAHs in these regions. In particular, the H atom energy dependence of the cross-sections for H atom addition and molecular hydrogen forming abstraction reactions as well as the cross-sections for UV induced hydrogen loss from super-hydrogenated PAHs must be determined.

Acknowledgements

We acknowledge financial support from the European Research Council under ERC starting grant “HPAH,” No. 208344 and the European Commission’s 7th Framework Programme through the “LASSIE” ITN under Grant Agreement Number 238258.

Notes and references

[a] Department of Physics and Astronomy and Intersciplinary Nanoscience Center (iNANO), Aarhus University, Ny Munkegade 120, 8000 Aarhus, Denmark. Fax: +45 8612 0740; Tel: +45 871 56336; E-mail: liv@phys.au.dk (LH).

[b] Current Address: Physikalisches Institut, Westfälische Wilhelms-Universität Münster, Germany.

Electronic Supplementary Information (ESI) available: See DOI: 10.1039/b000000x/

1 A. G. G. M. Tielens, *Rev. Mod. Phys.*, 2013, **85**, 1021-1081.
2 E. Habart, F. Boulanger, L. Verstraete, G. P. des Fortes, E. Falgarone and A. Abergel, *Astron. Astrophys.*, 2003, **397**, 623-634.
3 E. Habart, F. Boulanger, L. Verstraete, C. M. Walmsley and G. P. des Forets, *Astron. Astrophys.*, 2004, **414**, 531-544.
4 M.P. Bernstein, S.A. Sandford, and L.J. Allamandola, Ap. J. 1996, **472**, L127.
5 G. C. Sloan, J.D. Bregman, T.R. Geballe, L.J., Allamandola, Land C.E. Woodward,, Ap. J, 1997, **474**, 735.
6 V. Le Page, T.P. Snow, and V.M. Bierbaum, Ap. J. 2003, **584,** 316.
7 D.R. Wagner, H. Kim, and R.J. Saykally, Ap. J. 2000, **545**, 854C. W. Bauschlicher, *Astrophys. J. Lett.*, 1998, **509**, L125-L127.
8 V. Le Page, T. P. Snow and V. M. Bierbaum, *Astrophys. J.*, 2009, **704**, 274-280.
9 E. Rauls and L. Hornekær, *Astrophys. J.*, 2008, **679**, 531-536.
10 P. Cassam-Chena¨ı, F. Pauzat, & Y. Ellinger, 1994, in AIP Conf. Proc. 312.
11 Molecules and Grains in Space, ed. I. Nenner (Melville, NY: AIP), 543C.W. Bauschlicher, *Astrophys. J.*, 1998, **509**, L125.
12 Bernstein, M. P., Elsila, J. E., Dworkin, J. P., et al. *Astrophys. J.*, 2002, **576**, 1115.
13 V. Le Page, T.P. Snow, & V.M. Bierbaum, *Astrophys. J.*,. 2009, **704**, 274.
14 P. M. Goumans, Mon. Not. R. Astron. Soc., 2011, 415, 3129-3134.
15 T. P. Snow, V. Le Page, Y. Keheyan and V. M. Bierbaum, *Nature*, 1998, **391**, 259-260.
16 L. Boschman, G. Reitsma, S. Cazaux, T. Schlatholter, R. Hoekstra, M. Spaans and O. Gonzalez-Magana, *Astrophys. J. Lett.*, 2012, **761**, L33.
17 B. Klærke, Y. Toker, D. B. Rahbek, L. Hornekær and L. H. Andersen, *Astron. Astrophys.*, 2013, **549**, A84.
18 V. Mennella, L. Hornekær, J. Thrower and M. Accolla, *Astrophys. J. Lett.*, 2012, **745**, L2.
19 J. D. Thrower, B. Jørgensen, E. E. Friis, S. Baouche, V. Mennella, A. C. Luntz, M. Andersen, B. Hammer and L. Hornekær, *Astrophys. J.*, 2012, **752**, 3.
20 J. D. Thrower, E. E. Friis, A. L. Skov, B. Jørgensen and L. Hornekær. *Phys. Chem. Chem. Phys*. 2013, DOI: 10.1039/c3cp54073a
21 Y. Fu, J. Szczepanski, and N.C. Polfer, *Astrophys. J.*, 2012, **744**, 61.
22 E.L.O. Bakes and A.G.G.M. Tielens, *Astrophys. J.*, 1998, **499**, 258.
23 J.D. Bregman and P. Temi, *Astrophys. J.*, 2001, **554**, 126
24 J.E. Chiar, A.G.G.M. Tielens, D. C. B., Whittet et al. *Astrophys. J.*, 2000, **537**, 749
25 K. G. Tschersich and V. von Bonin, *J. Appl. Phys.*, 1998, **84**, 4065-4070.
26 K. G. Tschersich, *J. Appl. Phys.*, 2000, **87**, 2565-2573.
27 M. Bonfanti, S. Casolo, G.F. Tantardini and R. Martinazzo Phys. Chem. Chem. Phys., 2011, 13, 16680–16688.
28 J. D. Thrower, E. E. Friis, A. L. Skov, L. Nilsson, M. Andersen, L. Ferrighi, B. Jørgensen, S. Baouche, R. Balog, B.

Hammer and L. Hornekær, *J. Phys. Chem. C*, 2013, **117**, 13520-13529.

29 H. Cuppen and L. Hornekær, *J. Chem. Phys.,* 2008, **128**, 174707-13529.

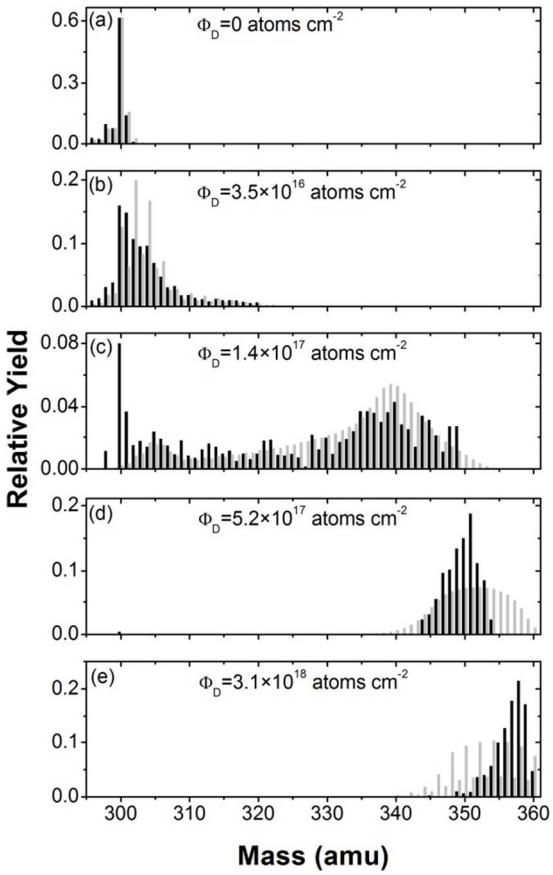

Figure 1: Experimental (black) and simulated (grey) mass distributions. The cross-sections used for the simulations are given in table 1 under simulation 1. Specifically, the abstraction cross-section per excess H/D atom, σ_{abs}, is fixed at the experimentally determined value for 300 K H atom beams: σ_{abs}=0.06 Å^2.

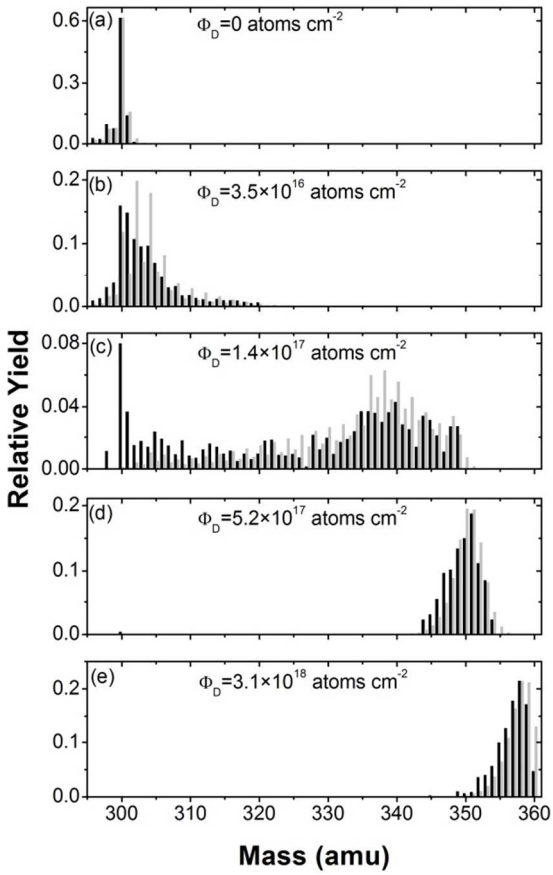

Figure 2: Experimental and simulated mass distributions using the cross-sections given in table 1 under simulation 2. σ_{abs}=0.01 Å^2 Has been used, since this value gives the best fit to the mass distributions at long exposures.

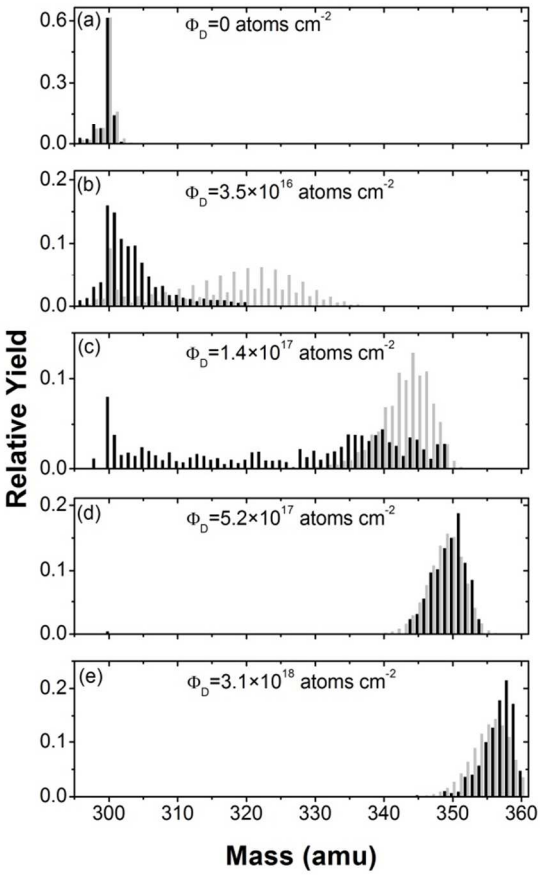

Figure 3: Experimental and simulated mass distributions using the cross-sections given in table 1, simulation 3. The addition cross-section have been chosen to depend linearly on the number of available sites for hydrogenation 0.15 Å^2*(24-n), σ_{abs}=0.01 Å^2.

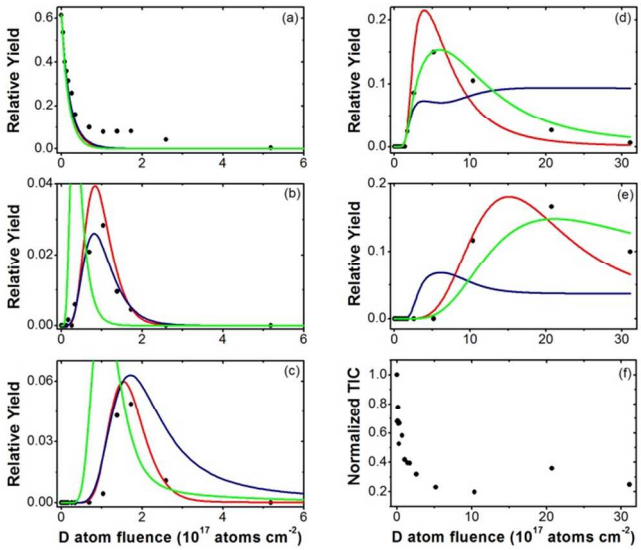

Figure 4: Evolution in the abundance of a) mass 300 amu, b) 320 amu, c) 340 amu, d) 350 amu and e) 355 amu as a function of D atom exposure. Black dots are experimental data, blue curves are simulation 1 (see Fig. 1) with a high abstraction cross-section, red curves are simulation 2 (see Fig. 2) with a lower abstraction cross-section, while green curves simulation 3 (see Fig. 3), with a constant cross-section pr. available addition site. f) Evolution of the total ion count.

Table 1: Abstraction (σ_{abs}) and addition ($\sigma_{add}(n)$) cross-sections used in the simulations displayed in Figures 1-3. All values are in units of Å^2.

	Simulation 1	Simulation 2	Simulation 3
σ_{abs}/site	0.06	0.01	0.01
$\sigma_{add}(0)$	0.55	0.55	0.55
$\sigma_{add}(1)$	0.55	0.55	3.45
$\sigma_{add}(2)$	0.55	0.55	3.30
$\sigma_{add}(3)$	1.00	1.00	3.15
$\sigma_{add}(4)$	2.50	2.00	3.00
$\sigma_{add}(5)$	2.50	2.00	2.85
$\sigma_{add}(6)$	2.50	2.00	2.70
$\sigma_{add}(7)$	2.50	2.00	2.55
$\sigma_{add}(8)$	2.50	2.00	2.40
$\sigma_{add}(9)$	2.50	2.00	2.25
$\sigma_{add}(10)$	2.50	2.00	2.10
$\sigma_{add}(11)$	2.50	2.00	1.95
$\sigma_{add}(12)$	2.50	2.00	1.80
$\sigma_{add}(13)$	2.50	2.00	1.65
$\sigma_{add}(14)$	2.50	2.00	1.50
$\sigma_{add}(15)$	2.50	2.00	1.35
$\sigma_{add}(16)$	2.50	2.00	1.20
$\sigma_{add}(17)$	2.50	2.00	1.05
$\sigma_{add}(18)$	1.30	1.00	0.90
$\sigma_{add}(19)$	1.30	1.00	0.75
$\sigma_{add}(20)$	1.30	1.00	0.60
$\sigma_{add}(21)$	1.30	1.00	0.45
$\sigma_{add}(22)$	1.30	1.00	0.30
$\sigma_{add}(23)$	1.30	1.00	0.15